SAND2007-3152C

OPTIMAL TURNING PATH GENERATION FOR UNMANNED AERIAL VEHICLES

Andrea Noonan*, Dale Schinstock*, Chris Lewis*, Barry Spletzer°
Kansas State University*; Sandia National Laboratories°
Manhttan, Kansas; Albuquerque, New Mexico, USA
alw4466@ksu.edu, dales@ksu.edu, clewis@ksu.edu, blsplet@sandia.gov

ABSTRACT
In this paper, we present an optimal method for calculating turning maneuvers for an unmanned aerial vehicle (UAV) developed for ecological research. The algorithm calculates several possible solutions using vectors represented in complex notation, and selects the shortest turning path given constraints determined by the aircraft. This algorithm considers the UAV's turning capabilities, generating a two-dimensional path that is feasible for the UAV to fly. We generate a test flight path and show that the UAV is capable of following the turn maneuvers.

KEY WORDS
Path planning, optimal turning, unmanned aerial vehicle

1. Introduction

Unmanned aerial vehicles (UAVs) have become increasingly common for both military and civilian applications. Autopilots are now commercially available for small aircraft, simplifying the development of an UAV. Typically, the navigation system of the autopilot in a UAV is provided with a series of waypoints defining a task for the UAV to complete. Using Cloud Cap Technology's Piccolo autopilot, researchers at Kansas State University developed a small UAV, named ECat. ECat, shown in Figure 1, is a hand-launched electric-powered UAV modified from a hobby-grade Sig Kadet airframe to incorporate a larger payload bay.

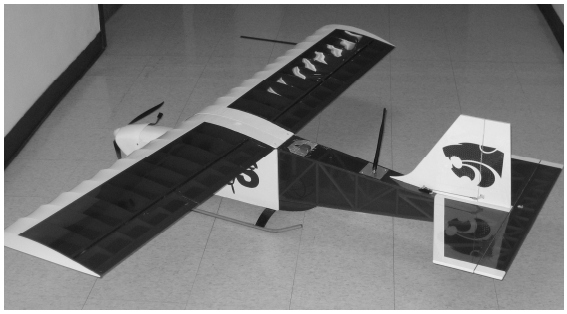

Figure 1: ECat UAV used for collecting data for environmental and agronomy research

Landing skids were also added to allow ECat to land in grassy fields. This system is being used to collect data for environmental and agricultural research. Typical missions require collecting image and multi-spectral data from test fields or prairie reserve wildlife areas.

Figure 2 depicts a typical mission where the ECat UAV must fly a grid over an area collecting images. At the end of each pass, the plane must maneuver to align itself for the next straight line segment. It is straightforward to define the waypoints for straight line segments. However, the autopilot often does not efficiently reverse directions, align itself for the next pass, and track the path well on its own. To provide for efficient turning, the autopilot navigator code on ECat was modified to perform turn maneuvers consisting of arc and straight line segments. This paper describes a closed form method for automatically generating these arcs and lines that minimizes the time required for turning and realignment maneuvers. The solution generates smooth trajectories that align the UAV for its next segment while taking into account the aircraft's limited turning capabilities.

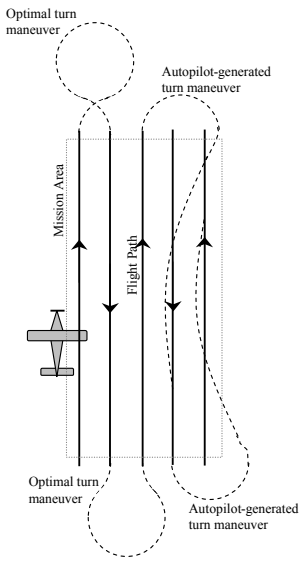

Figure 2: A general flight path for an ECat mission over a field

Similar work was done by Anderson, et al [1] and they offer a solution to the re-alignment problem. However, their solution requires iteratively solving a set of differential equations whereas our solution is closed form. Other path planning methods, such as [2], determine waypoints on a course through a dangerous area based on risk assessment algorithms, but do not necessarily take the vehicle's turning capabilities into account. Whang and Hwang describe a method for smoothing flight path trajectories in [3], but relax the constraint that the vehicle passes through specified waypoints. Yang and Kapila address optimal path planning in [4], describing method similar to [1] and this work, but do not address three-arc turning paths. Other methods such as those in [3] and [5] find a minimum length path by minimizing a cost function. In this paper, we assume the solution to the optimization problem and present a means of algebraically calculating it. Dubins [6] proves that a solution involving either three arcs of a minimum radius or two arcs and a line is optimal.

In this paper, we present a method for generating an optimum turning maneuver. The method expresses the path as a set of complex vector equations which are then solved in closed form to generate an optimal path. To demonstrate the effectiveness of our procedure, we used ECat to fly a path generated using the method described here. The resulting flight data clearly demonstrates the efficacy of the method. The remainder of this paper is as follows. First, in Section II, we derive the optimum turn maneuver in closed form. In Section III we show simulation and real flight data. Finally our conclusions are discussed in Section IV.

2. Problem Statement and Solution

There exist an infinite number of trajectories which maneuver the aircraft from an arbitrary initial position and heading to another arbitrary final position and heading while maintaining constant speed and altitude. Our goal is to select a two-dimensional path which minimizes the time of the maneuver. Typically, minimum time optimizations result in maximum control inputs. Based on this fact and heuristic arguments, we conclude that an optimal maneuver consists of a sequence of segments of either maximum left- or right-handed arcs or straight lines. Figure 3 demonstrates that the initial and final segment of an optimal maneuver will always be an arc segment. It also demonstrates that the optimal maneuver can be accomplished with at most three segments. Sometimes the middle segment can be a straight line and sometimes it is another arc. Up to eight unique possible paths can be generated using combination of maximum left- or right- handed turns and line segments. Our algorithm generates all possible paths of this type, and then selects the shortest one.

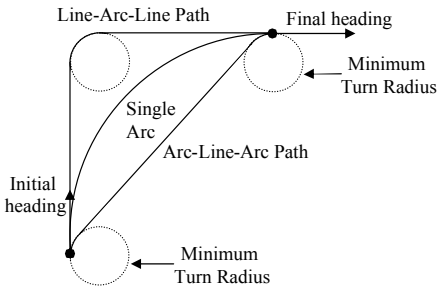

Figure 3: Comparison of different path types

2.1 Three-Turn Solutions

Referring to Figure 4, we show an arbitrary three-turn solution. The initial and final headings are known and denoted as θ_i and θ_f. The unknown subtended angles of each arc are θ_A, θ_B, and θ_C. The points $\vec{A}$, $\vec{B}$, and $\vec{C}$ are the centers of the arcs and $\vec{D}$ is the destination position. We scale all distance measurements to the turn radius, i.e., one unit equals the turn radius.

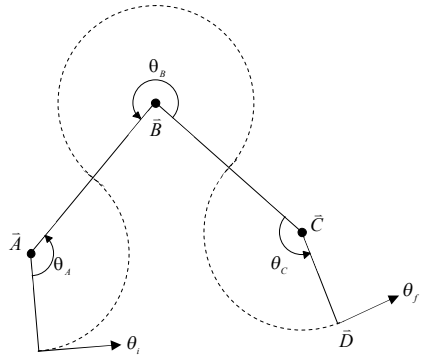

Figure 4: An arbitrary 3-turn solution

Taking the start of the first turn as the origin of the coordinate system, without loss of generality, we can represent this path as the sum of five complex vectors as follows:

$$e^{j\cdot\left(\theta_i+s\cdot\frac{\pi}{2}\right)}+2\cdot e^{j\cdot\left(\theta_i+s\cdot\left(\theta_A-\frac{\pi}{2}\right)\right)}+2\cdot e^{j\cdot\left(\theta_i+s\cdot\left(\frac{\pi}{2}+\theta_A-\theta_B\right)\right)} = \left|\vec{D}\right|\cdot e^{j\theta_D}+e^{j\cdot\left(\theta_f+s\cdot\frac{\pi}{2}\right)} \quad (1)$$

where *s* denotes the direction of the starting turn and is equal to +1 for a CCW turn or -1 for a CW turn. Simplifying (1) by rotating by $-\theta_i$ and by $s\frac{\pi}{2}$, rearranging the equation, and noting that $e^{is\pi}=-1$ regardless of *s* we get

$$e^{j\cdot s\cdot\theta_A}-e^{j\cdot s\cdot(\theta_A-\theta_B)}=\frac{1}{2}\left[\left|\vec{D}\right|\cdot e^{j\cdot\left(\theta_D-\theta_i+s\frac{\pi}{2}\right)}-e^{j\cdot(\theta_f-\theta_i)}+1\right]. \quad (2)$$

Since the right hand side of (2) is known, the equation can be rewritten in the following form:

$$e^{j\cdot s\cdot\theta_A} - e^{j\cdot s\cdot(\theta_A-\theta_B)} = G\cdot e^{j\cdot\theta_G} \qquad (3)$$

where

$$G\cdot e^{j\cdot\theta_G} = \frac{1}{2}\left[\left|\vec{D}\right|\cdot e^{j\cdot\left(\theta_D-\theta_i+s\frac{\pi}{2}\right)} - e^{j\cdot(\theta_f-\theta_i)} + 1\right]. \qquad (4)$$

Rotating by $-\theta_G$, equation (3) can be rewritten as

$$e^{j\cdot a} - e^{j(a+b)} = G\cdot e^{j\cdot 0} \qquad (5)$$

where

$$\begin{aligned} a &= s\theta_A - \theta_G \\ b &= -s\theta_B \end{aligned}. \qquad (6)$$

From (4) there are two values for G and θ_G corresponding to (G_1,θ_{G_1}) for $s=1$ and (G_2,θ_{G_2}) for $s=-1$. If $G>2$ then (5) has no solution and a straight line solution is needed. This situation will be addressed in the next section. Otherwise, we may solve for the two unknowns *a* and *b* using Euler's identity and equating real and imaginary parts of (5) as follows:

$$\cos(a)-\cos(a+b)=G \qquad (7)$$

and

$$\sin(a)=\sin(a+b). \qquad (8)$$

Equation (7) reduces to

$$b = 2n\pi \qquad (9)$$

where *n = 0, 1, 2, ...* or

$$b=(2n+1)\pi - 2a\,. \qquad (10)$$

Equation (9) is an obvious solution of (8), and represents the case where a single arc is sufficient to optimally complete the maneuver. This case will be handled in the Two-Turn solution when the line length equals zero and the subtended angle for this situation will be equal to $\theta_f-\theta_i$. Otherwise, equation (10) applies. Substituting (10) into (7), and simplifying yields four solutions for a:

$$\begin{aligned} a_1 &= +\cos^{-1}\left(G_1/2\right) \\ a_2 &= +\cos^{-1}\left(G_2/2\right) \\ a_3 &= -\cos^{-1}\left(G_1/2\right) \\ a_4 &= -\cos^{-1}\left(G_2/2\right) \end{aligned}. \qquad (11)$$

Substituting (11) into (6) yields the angles θ_A, θ_B. Noting that θ_C is dependent on the difference between θ_f and θ_i as well as the angles θ_A and θ_B, we have $\theta_f-\theta_i = s(\theta_A-\theta_B+\theta_C)$. Solving for θ_A, θ_B and θ_C we have

$$\begin{aligned} \theta_{A_1} &= +(a_1+\theta_{G_1}), \quad \theta_{B_1} = +(2a_1-\pi), \\ \theta_{C_1} &= +(\theta_f-\theta_i+a_1-\pi-\theta_{G_1}) \\ \theta_{A_2} &= -(a_2+\theta_{G_2}), \quad \theta_{B_2} = -(2a_2-\pi), \\ \theta_{C_2} &= -(\theta_f-\theta_i+a_2-\pi-\theta_{G_2}) \\ \theta_{A_3} &= +(a_3+\theta_{G_1}), \quad \theta_{B_3} = +(2a_3-\pi), \\ \theta_{C_3} &= +(\theta_f-\theta_i+a_3-\pi-\theta_{G_1}) \\ \theta_{A_4} &= -(a_4+\theta_{G_2}), \quad \theta_{B_4} = -(2a_4-\pi), \\ \theta_{C_4} &= -(\theta_f-\theta_i+a_4-\pi-\theta_{G_2}) \end{aligned}. \qquad (12)$$

Since values for θ_A, θ_B, and θ_C greater than 2π do not provide an optimal solution, we restrict all the magnitude of all angles to be between 0 and 2π.

2.2 Two Turn Solutions with Straight Line Segment

As mentioned the previous subsection, if $G>2$, then a straight line solution is needed. Also, there are some solutions where $G<2$ and a straight line is a part of the shortest path. In order for a straight line solution to occur, the heading at the end of the initial turn and at the beginning of the final turn must be the same. When $G=2$, a single arc is sufficient to complete the turn. Regardless of whether the initial and final turns are in the same direction or in opposite directions, the two-turn solutions are calculated the same way.

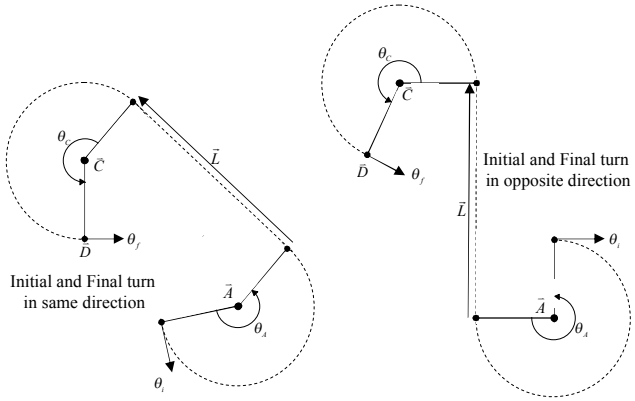

Figure 5: Two turn plus straight line situations

Similar to the solution method in Section 2.1, we refer to Figure 5 and write a vector loop equation

$$e^{j\cdot\left(\theta_i+s_1\pi/2\right)} + e^{j\cdot\left(\theta_i-s_1\pi/2+\theta_A\right)} + L\cdot e^{j\cdot(\theta_i+\theta_A)} + e^{j\cdot\left(\theta_i+\theta_A+s_2\pi/2\right)} = D\cdot e^{j\cdot\theta_D} + e^{j\cdot\left(\theta_f+s_2\pi/2\right)}. \qquad (13)$$

Here s_1 denotes the direction of the initial turn and s_2 is the direction of the final turn. Rearranging (13) we have

$$D \cdot e^{j\cdot\theta_D} + e^{j\cdot\left(\theta_f + s_2\pi/2\right)} - e^{j\cdot\left(\theta_i + s_1\pi/2\right)} = e^{j\cdot\left(\theta_i - s_1\pi/2 + \theta_A\right)} + L \cdot e^{j\cdot(\theta_i+\theta_A)} + e^{j\cdot\left(\theta_i+\theta_A+s_2\pi/2\right)} \quad (14)$$

or

$$G \cdot e^{j\cdot\theta_G} = e^{j\cdot\left(\theta_i - s_1\pi/2 + \theta_A\right)} + L \cdot e^{j\cdot(\theta_i+\theta_A)} + e^{j\cdot\left(\theta_i+\theta_A+s_2\pi/2\right)} \quad (15)$$

where

$$G \cdot e^{j\cdot\theta_G} = D \cdot e^{j\cdot\theta_D} + e^{j\cdot\left(\theta_f + s_2\pi/2\right)} - e^{j\cdot\left(\theta_i + s_1\pi/2\right)}. \quad (16)$$

There are up to four possible two turn solutions:

$$\begin{aligned} s_1 &= +1, \quad & s_2 &= +1 \\ s_1 &= -1 \quad & s_2 &= -1 \\ s_1 &= +1, \quad & s_2 &= -1 \\ s_1 &= -1 \quad & s_2 &= +1 \end{aligned} \quad \textbf{(17)}$$

We will look the cases $s_1 = s_2$ and $s_1 = -s_2$ separately.

First, we let $s_1 = s_2$, then the first and third terms on the right-hand side of (15) represent vectors of equal magnitudes pointing in opposite directions. Therefore these terms cancel and we have

$$G \cdot e^{j\cdot\theta_G} = L \cdot e^{j\cdot(\theta_i+\theta_A)}. \quad (18)$$

For two vectors to be equal, both the magnitude and direction must be equal. Therefore

$$G = L \quad (19)$$

and

$$\theta_A = \theta_G - \theta_i \quad (20)$$

for $s_1 = s_2$. Since G will has two values (one for $s_1 = s_2 = +1$ and $s_1 = s_2 = -1$), θ_A will have two values

Now let $s_1 = -s_2$. The first and third terms on the right-hand side of (15) are vectors of equal length pointing in the same direction. Thus (15) becomes

$$G \cdot e^{j\cdot\theta_G} = 2e^{j\cdot\left(\theta_i + s_2\pi/2 + \theta_A\right)} + L \cdot e^{j\cdot(\theta_i+\theta_A)}. \quad (21)$$

Rotating (21) by $-\theta_i - \theta_A$ we have

$$G \cdot e^{j\cdot(\theta_G - \theta_i - \theta_A)} = 2e^{j\cdot\left(s_2\pi/2\right)} + L \cdot e^{j\cdot(0)}. \quad (22)$$

Using Euler's identity and simplifying yields

$$G\cos\left(\theta_G - \theta_i - \theta_A\right) = L \quad (23)$$

and

$$G\sin\left(\theta_G - \theta_i - \theta_A\right) = 2\sin\left(s_2\,\pi/2\right). \quad (24)$$

Since $2\sin\left(s_2\,\pi/2\right)$ will equal -1 for $s_2 = -1$ and 1 for $s_2 = +1$ we can write

$$G\sin\left(\theta_G - \theta_i - \theta_A\right) = 2s_2. \quad (25)$$

We can solve for θ_A by dividing equation (25) by (23) and simplify to get

$$\theta_A = \theta_G - \theta_i - \tan^{-1}\left(\frac{2s_2}{L}\right) \quad (26)$$

and we can square (23) and (25), add the result together and rearrange to get

$$L = \sqrt{G^2 - 2^2}. \quad (27)$$

Since L represents a magnitude, the negative solution in (27) is invalid. If $G \geq 2$, then L can be determined. If $G = 2$, then $L = 0$ and a single arc completes the turn maneuver. These equations are valid if $s_1 = -s_2$.

From equations (20) and (26), we have values for θ_A. Referring to Figure 5 we can add angles to get $\theta_i + \theta_A + \theta_C = \theta_f$ or rewriting this we have

$$\theta_C = \theta_f - \theta_i - \theta_A \quad (28)$$

and we have four solutions sets for $[\theta_A, \theta_C]$:

$$\begin{aligned} \theta_{A_1} &= \theta_{G(s_1=s_2=+1)} - \theta_i, \\ \theta_{C_1} &= \theta_f - \theta_i - \theta_{A_1} \\ \theta_{A_2} &= \theta_{G(s_1=s_2=-1)} - \theta_i, \\ \theta_{C_2} &= \theta_f - \theta_i - \theta_{A_2} \\ \theta_{A_3} &= \theta_{G(s_2=-s_1=+1)} - \theta_i - \tan^{-1}\left(\frac{2}{L}\right), \\ \theta_{C_3} &= \theta_f - \theta_i - \theta_{A_3} \\ \theta_{A_4} &= \theta_{G(s_2=-s_1=-1)} - \theta_i - \tan^{-1}\left(\frac{-2}{L}\right), \\ \theta_{C_4} &= \theta_f - \theta_i - \theta_{A_4} \end{aligned} \quad (29)$$

where θ_G is calculated from (16) using the indicated values for s_1 and s_2.

2.3 The Quickest Solution.

There are up to eight possible solutions for any turn maneuver – up to 4 three-turn solutions and up to 4 two-turn plus line segment solutions. Since we want the quickest (i.e. shortest) path, we need to pick the quickest solution. For the three-turn solutions, since all the turn radii are equal, we can add θ_A, θ_B, and θ_C together for each solution and choose the minimum sum. (We must

also keep track of which thetas give the quickest three-turn solution.)

All units in the preceding equations are normalized to the turn radius, thus one unit of linear travel is equal to one unit (i.e. radian) of angular travel. We find $\theta_A + \theta_C + |L|$ for each two-turn plus line segment solution, choose the smallest sum, and keep track of the thetas and lengths that comprise the minimum sum. At this point, we have determined the shortest three-turn solution and the shortest two-turn plus line segment solution.

Comparing $\theta_A + \theta_B + \theta_C$ and $\theta_A + \theta_C + |L|$, we choose the smallest sum to get the minimum overall solution. If the three-turn solution is the quickest, we choose Θ_A, Θ_B, and Θ_C to correspond to θ_A, θ_B, and θ_C from the quickest three-turn solution. If the two-turn solution is quickest, we choose Θ_A and Θ_C to correspond to θ_A and θ_C from the quickest two-turn solution and select $\Theta_B = |L_{\min}|$ where $L_{\min}$ is the line segment from the shortest two-turn solution.

Figure 6 provides a summary of the algorithm.

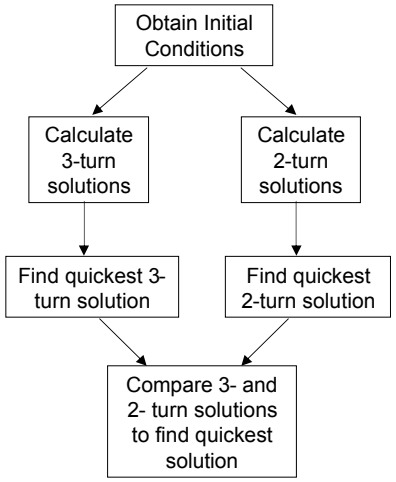

Figure 6: Algorithm summary

3. Example, Simulation, and Flight Test

3.1 Algorithm Example

In this section, we use the method described in Section 2 to demonstrate the results of the optimal turning algorithm. We begin with initial conditions:

$$\theta_i = \frac{\pi}{2}, \qquad \theta_f = -\frac{\pi}{2} \qquad (30)$$
$$\theta_D = 0, \qquad D = 35$$

where the angles are in radians and D is in meters. Since the autopilot's bank angle limit is 30 degrees, we set the maximum bank angle needed to track the path at 15 degrees. This will allow the autopilot to have authority to correct the UAV's position. For the 15 degree bank angle and a 15 m/s velocity, it can be shown, assuming a coordinated turn, that the minimum turning radius, R of the UAV will be approximately 85 meters. Given these initial conditions, the algorithm was used to calculate six possible solutions shown in Figure 7. Clearly some solutions in the figure have longer path lengths than others. Calculating the quickest solution confirms that the 3-Turn Solution 4 is the shortest path for the given initial conditions. Using this turning maneuver, we assembled a flight path for simulation and flight testing. These test results are discussed in the following sections.

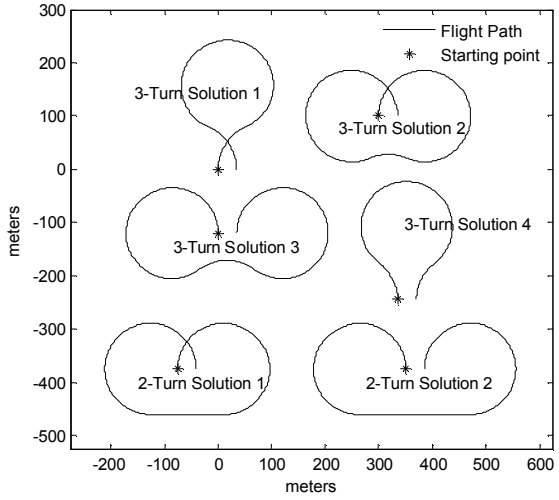

Figure 7: Six possible turning solutions calculated for the conditions given the in example

3.2 Simulation and Flight Test Results

Using the optimal turn maneuver result from the previous section, we rotated the turning path and constructed a "bulbous racetrack" flight path as shown in Figures 8 and 9. Ten waypoints were used to describe the flight path: three arc waypoints for each complete turn maneuver, and four waypoints to describe the lines connecting the turning maneuvers.

The flight plan was first tested in simulation. Figure 8 shows a plot of this test. The UAV simulation tracked the path reasonably well. We believe that the tracking errors are due to problems inside the navigator and will be addressing them in future work.

The same path was also flown with the ECat UAV in an open area near Manhattan, KS on a day with little wind. The ECat was remotely piloted for take-off and landing, and the same autopilot used for the simulation was used. Figure 9 shows the desired flight path along with the results of the flight test. Only the autopilot-controlled section of the flight is displayed to avoid cluttering the figure.

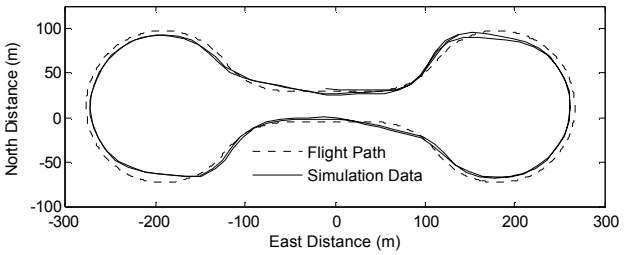

Figure 8: Simulation flight of optimal turn path.

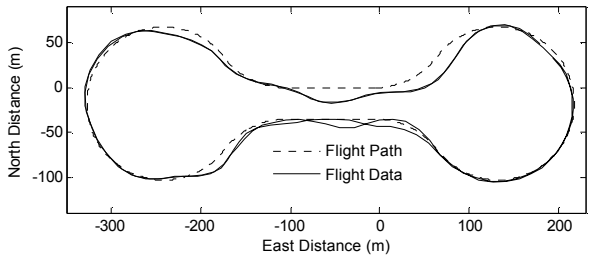

Figure 9: Actual flight of optimal turn path.

4. Conclusions

A closed-from method for generating turning maneuvers for a UAV was developed. This method assumes that the solution will consist of full right- or left-handed turns and utilizes vectors represented in complex form. This method determines the quickest turning maneuver for a given situation, and is easily implemented in software. The aircraft's turning capabilities are also taken into account with this method, resulting in a feasible UAV trajectory. To test the turning maneuver algorithm, a simulation flight and an actual test flight in an open area were performed. These flight tests showed that the UAV is able to fly paths generated with the method presented here. Future work includes combining the turn maneuvers with path segments to generate complete paths for an entire UAV mission.

References

[1] E.P. Anderson, R.W. Beard, & T.W. McLain, Real-time dynamic trajectory smoothing for unmanned air vehicles, *IEEE Trans. of Control Systems Technology*, *13*(3), 2005, 471-477.

[2] D. Gu, W. Kaml, & I. Postlethwaite, A UAV waypoint generator, *AIAA 1st Intelligent Systems Technical Conf.*, Chicago, IL, 2004, 1-6.

[3] I. H. Whang, & T. W. Hwang, Horizontal waypoint guidance design using optimal control, *IEEE Trans. on Aerospace and Electronic Systems*, *38*(3), 2002, 1116-1120.

[4] Yang, G. & V. Kaplia, Optimal path planning for unmanned air vehicles with kinematic and tactical constraints, *Proc. 41st IEEE Conf. on Decision and Control*, Las Vegas, NV, 2002, 1301-1306.

[5] G. Moon, & Y. Kim, Flight path optimization passing through waypoints for autonomous flight control systems, *Engineering Optimization*, *37*(7), 2005, 755-774.

[6] L. E. Dubins, On curves of minimal length with a constraint on average curvature and with prescribed initial and terminal positions and tangents, *American Journal of Mathematics*, *79*(3), 1957, 497-516.